doi:10.1093/brain/awr161 Brain 2011: 134; 2248–2260 | 2248

BRAIN
A JOURNAL OF NEUROLOGY

# The contribution of gliosis to diffusion tensor anisotropy and tractography following traumatic brain injury: validation in the rat using Fourier analysis of stained tissue sections

**Matthew D. Budde,[1,2,3] Lindsay Janes,[2] Eric Gold,[2] Lisa Christine Turtzo[2] and Joseph A. Frank[1,2,4]**

1 Radiology and Imaging Sciences, Clinical Centre, National Institutes of Health, Bethesda, MD, 20892 USA
2 Center for Neuroscience and Regenerative Medicine, Uniformed Services University of the Health Sciences, Bethesda, MD, 20814 USA
3 Department of Neurosurgery, Medical College of Wisconsin, Milwaukee, WI, 53226 USA
4 National Institute of Biomedical Imaging and Bioengineering, National Institutes of Health, Bethesda, MD, 20892 USA

Correspondence to: Matthew Budde,
8701 Watertown Plank Rd,
C1890 Neuroscience Research Centre,
Milwaukee WI 53226, USA
E-mail: mdbudde@mcw.edu

**Diffusion tensor imaging is highly sensitive to the microstructural integrity of the brain and has uncovered significant abnormalities following traumatic brain injury not appreciated through other methods. It is hoped that this increased sensitivity will aid in the detection and prognostication in patients with traumatic injury. However, the pathological substrates of such changes are poorly understood. Specifically, decreases in fractional anisotropy derived from diffusion tensor imaging are consistent with axonal injury, myelin injury or both in white matter fibres. In contrast, in both humans and animal models, increases in fractional anisotropy have been suggested to reflect axonal regeneration and plasticity, but the direct histological evidence for such changes remains tenuous. We developed a method to quantify the anisotropy of stained histological sections using Fourier analysis, and applied the method to a rat controlled cortical impact model to identify the specific pathological features that give rise to the diffusion tensor imaging changes in subacute to chronic traumatic brain injury. A multiple linear regression was performed to relate the histological measurements to the measured diffusion tensor changes. The results show that anisotropy was significantly increased ($P < 0.001$) in the perilesioned cortex following injury. Cortical anisotropy was independently associated (standardized $\beta = 0.62$, $P = 0.04$) with the coherent organization of reactive astrocytes (i.e. gliosis) and was not attributed to axons. By comparison, a decrease in white matter anisotropy ($P < 0.001$) was significantly related to demyelination ($\beta = 0.75$, $P = 0.0015$) and to a lesser extent, axonal degeneration ($\beta = -0.48$, $P = 0.043$). Gliosis within the lesioned cortex also influenced diffusion tensor tractography, highlighting the fact that spurious tracts in the injured brain may not necessarily reflect continuous axons and may instead depict glial scarring. The current study demonstrates a novel method to relate pathology to diffusion tensor imaging findings, elucidates the underlying mechanisms of anisotropy changes following traumatic brain injury and significantly impacts the clinical interpretation of diffusion tensor imaging findings in the injured brain.**

**Keywords:** anisotropy; traumatic brain injury; gliosis; axonal degeneration; diffusion tensor imaging

**Abbreviations:** $A_{er}$ = anisotropy index eigenvalue ratio; DiI = 1,1′-dioctadecyl-3,3,3′3′-tetramethylindocarbocyanine perchlorate; DTI = diffusion tensor imaging; MAP2 = microtubule-associated protein 2; SMI = Sternberger monoclonal antibody

Received April 15, 2011. Revised May 23, 2011. Accepted June 1, 2011. Advance Access publication July 15, 2011

# Introduction

Traumatic brain injury is an important public health problem affecting over 2.5 million people worldwide (Cox *et al.*, 2011). It encompasses a spectrum of injury from mild concussion to severe trauma with neurological sequelae that include cognitive deficits to debilitating impairment. Persistent long-term functional recovery from CNS trauma is limited, and there are no effective clinical treatments for traumatic brain injury. However, the potential for spontaneous recovery and improvement of function exists and is associated with intrinsic mechanisms of axonal plasticity, sprouting or regeneration (Cafferty *et al.*, 2008), each of which represent potential targets for therapeutic or rehabilitative intervention. Understanding the nature of these processes is important due to their tremendous clinical significance. However, evaluating these changes non-invasively in individual patients is a formidable challenge in which diffusion tensor imaging (DTI), an advanced MRI technique, has shown tremendous potential in delineating brain and spinal cord pathology.

DTI is unique in its ability to probe the microstructure of the nervous system non-invasively and has revealed abnormalities following traumatic brain injury not realized through other imaging techniques, including conventional relaxivity-based magnetic resonance or CT (Kim and Gean, 2011). In this regard, DTI is hoped to improve diagnosis and prognosis in patients with traumatic brain injury. Fractional anisotropy is a measure derived from DTI that reflects the coherent microscopic organization of axons. As such, it is highly specific for white matter fibres and is sensitive to subtle changes in the microstructural integrity. Following traumatic brain injury, fractional anisotropy is largely decreased (Arfanakis *et al.*, 2002), indicative of axonal degeneration and demyelination within injured white matter fibres that disrupts the coherent microstructure (Concha *et al.*, 2006). Occasionally, increased fractional anisotropy is observed in patients with traumatic brain injury (Voss *et al.*, 2006; Wilde *et al.*, 2008; Lo *et al.*, 2009) as well as in animal models (Jiang *et al.*, 2011). This is often interpreted as axonal regrowth or regeneration. However, the evidence for such changes remains tenuous due to the lack of direct, quantitative comparisons between DTI results and histological preparations. Moreover, a dominant feature of most traumatic injury is the formation of a glial scar by reactive astrocytes. Along with myelin-associated proteins, the glial scar inhibits neurite regrowth (Bush *et al.*, 1999). The contribution of the glial scar to the DTI changes in the injured brain has largely been ignored although it has significant implications in the determination of functional recovery, or lack thereof, in patients with traumatic brain injury.

In this report, we develop and apply a method to directly and quantitatively assess the anisotropic properties of stained histological sections and compare the results with DTI measurements in a rat model of traumatic brain injury. We demonstrate that increased anisotropy in the injured cortex is associated with coherent astrocyte reactivity and the formation of a glial scar rather than axonal regeneration. In contrast, the decreased anisotropy of the injured white matter is associated with both axonal degeneration and demyelination. The results demonstrate that the features that give rise to the anisotropy in the normal brain, particularly the axonal membrane (Beaulieu, 2002), are not necessarily the sole determinates of anisotropy in the injured brain. The results greatly impact the possible interpretation of DTI changes in the clinical setting of brain and spinal cord injury.

# Materials and methods

## Animal procedures

All animal procedures were approved by the animal studies committee at our institution. Eight to 12-week-old female Wistar rats ($n = 5$) were obtained from Charles River Laboratories and underwent a controlled cortical impact model of traumatic brain injury (Brody *et al.*, 2007). Animals were anaesthetized with isofluorane and placed in a stereotaxic holder. A craniotomy was performed by making an incision in the scalp and removing a 6-mm diameter bone flap centred at +1 mm and 2.5 mm lateral to bregma. The dura was left intact. A 5-mm impactor tip connected to an electromagnetic piston (Leica Microsystems) was used to deliver the controlled cortical impact at a depth of 2 mm, a velocity of 5 m/s and a dwell time of 100 ms. The bone flap was replaced and secured with dental acrylic and the scalp was sutured. Five naïve rats served as controls.

## Magnetic resonance imaging

*In vivo* DTI was performed at 2 months post controlled cortical impact on a 7 T Bruker Biospec (Bruker BioSpin) interfaced with Paravision 5.0. Animals were anaesthetized with isofluorane, placed in a magnetic resonance-compatible head holder and positioned in a 40-mm inner diameter Litz coil (Doty Scientific). Following the acquisition of gradient echo scout images, 15 coronal consecutive slices at a thickness of 0.5 mm were centred over the lesion at a resolution of $234 \times 234\ \mu m^2$. A multiple-echo pulsed gradient spin echo sequence (repetition time/echo time = 2250/19 ms; 4 echoes) was used to acquire three unweighted ($b = 0\ s/mm^2$) images and 15 diffusion weighted images ($b = 800\ s/mm^2$) using a Stejskal–Tanner diffusion preparation with parameters of $\Delta = 10$ ms and $\delta = 5$ ms. The full *in vivo* MRI experiment took ~2 h per animal. *Ex vivo* DTI was performed on a vertical bore 7 T Bruker with a microimaging gradient insert and a 20-mm probe. Fixed and excised brains were immersed in Fomblin (Solvay Solexis, Inc.) to prevent dehydration during the 20-h experiment. The same sequence was used to acquire five unweighted and 30 diffusion weighted images ($b = 1200\ s/mm^2$) with a slice thickness of 0.5 mm and a resolution of $156 \times 156\ \mu m^2$ with the following parameters: repetition time/echo time = 4000/20 ms, $\Delta = 10$ ms, $\delta = 4$ ms and number of averages = 4.

## Diffusion tensor imaging data analysis

The diffusion tensor was calculated using a linear least squares fit to the equation $S_i = S_0 * exp(-bD)$ on a pixel-by-pixel basis. Summary parameters, including fractional anisotropy, axial diffusivity ($\lambda_{\parallel} = \lambda_1$) and radial diffusivity [$\lambda_{\perp} = (\lambda_2 + \lambda_3)/2$], were derived, where $\lambda_1$, $\lambda_2$ and $\lambda_3$ are the largest to smallest eigenvalues. Regions of interest were traced on the $T_2$-weighted images separately for white and grey matter from the perilesioned, contralateral and control cortices, as shown in Fig. 1.

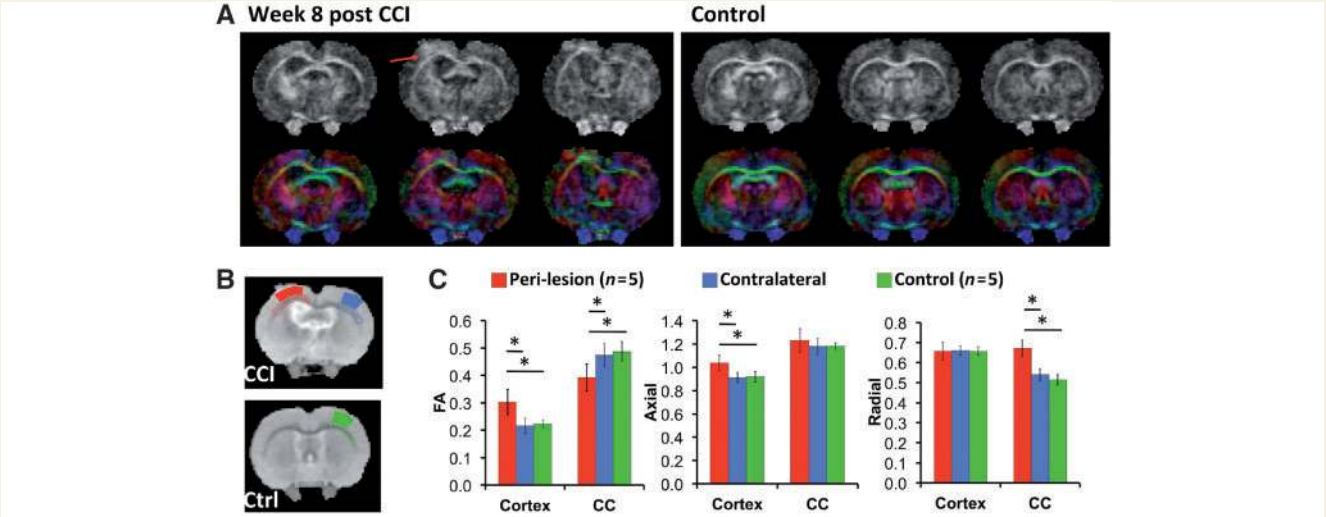


**Figure 1** *In vivo* DTI following controlled cortical impact in the rat brain. (**A**) A region of increased fractional anisotropy (FA) is observed in the perilesion cortex with its orientation maintained perpendicular to the cortical surface. (**B**) Regions of interest were placed on the $T_2$-weighted images in the perilesion, contralateral and control cortices and white matter for quantification. (**C**) In five controlled cortical impact and five naïve control animals, the significant increase in perilesion cortical fractional anisotropy was the result of an increase in axial (parallel) diffusivity with no change in radial (perpendicular) diffusivity. In the white matter, the decreased perilesion fractional anisotropy was a result of an increase in radial diffusivity with no change in axial diffusivity. Values indicate mean ± SD ($n = 5$ for each). *$P < 0.05$. CC = corpus callosum; CCI = controlled cortical impact.

## Histological preparation and imaging

Animals were perfused with phosphate buffered saline through the left ventricle followed by 4% paraformaldehyde in phosphate buffered saline. Brains were immersed in fixative overnight, cryoprotected in 30% sucrose overnight, embedded in optimal cutting temperature media and frozen in liquid nitrogen. Cryosectioning was performed at a thickness of 8 μm. Immunofluorescent staining was performed by rinsing sections three times in phosphate buffered saline, blocking for 5 min and incubating with the primary antibody at a 1:200 dilution overnight at 4°C. Sections were rinsed three times in phosphate buffered saline and incubated with the secondary antibody at 1:200 for 30 min at room temperature. Sections were rinsed three times and mounted with Vectashield®. Primary antibodies included antibodies against glial fibrillary acidic protein (Chemicon, MAB360), myelin basic protein (Abcam, ab24567), microtubule-associated protein 2 (MAP2; Sigma, M4403), phosphorylated neurofilaments (Covance, SMI31) and non-phosphorylated neurofilaments (Covance, SMI32). Sections were imaged using a confocal laser scanning microscope (LSM710, Carl Zeiss Microimaging) with a ×20 objective and an image size of 2048 × 2048, yielding a nominal resolution of 0.42 $\mu m^2$/pixel. The excitation intensity and gain settings were constant among sections stained with the same primary antibody. Selected sections were stained with the lipophilic cyanine dye 1,1′-dioctadecyl-3,3,3′3′-tetramethylindocarbocyanine perchlorate (DiI). Sections were dehydrated through a graded ethanol series (30–100%), rinsed for 10–20 s in 0.25 mg/ml DiI in 100% ethanol, rehydrated through graded ethanols, mounted and coverslipped. DiI-stained sections were imaged in their entirety using the montage feature on a stage-scanning epifluorescent microscope (Axio Imager, Carl Zeiss Microimaging) using a ×10 objective at a nominal resolution of 0.65 $\mu m^2$/pixel.

## Quantitative histology

The maps of microscopic anisotropy and orientation were derived using custom routines developed in Matlab (The Mathworks Inc.) as shown in Fig. 2 and described in Appendix I. Briefly, each image was subsampled into regions of 200 × 200 pixels. After filtering with a Tukey window ($\alpha = 0.4$) and zero mean normalizing to minimize edge and centre spike effects (Ayres *et al.*, 2008), respectively, the 2D fast Fourier transform was applied. A radial histogram was computed with a radial bin size of 10° followed by principal component analysis to derive the anisotropy and primary orientation as specified in Appendix I. Regions of interest encompassing the cortex or white matter were traced on the histological images at their native resolution and down-sampled to the lower resolution parameter maps. Although $A_{er}$ (anisotropy index eigenvalue ratio) is independent of image intensity, low levels of staining intensities inherent in different regions can bias the measured anisotropy (Pierpaoli and Basser, 1996; Armitage and Bastin, 2000). Therefore, $A_{er}$ values derived from each region of interest were scaled by the mean region of interest intensity normalized to the mean intensity of all sections of the same stain. As a consequence, scaled $A_{er}$ values reflect both anisotropy and relative staining intensity.

## Tractography

Diffusion tensor tractography was performed using the fibre assignment by the continuous tracking algorithm implemented in the Diffusion Toolkit (Wang *et al.*, 2007) with a fractional anisotropy threshold of 0.3. Regions of interest to quantify tractography results were created as shown in Fig. 2B and C. Pixels within a Euclidean distance of 234–702 μm (1–3 pixel widths) of the cortical surface were segmented with the medial and ventral aspects at the edges of

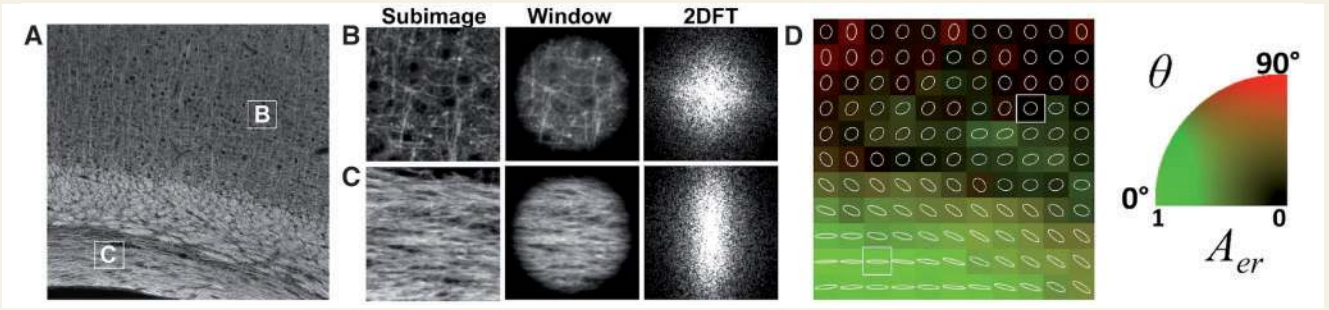


**Figure 2** Quantification of anisotropy in histological sections. (**A**) A brain section stained with DiI is shown from a control animal at the region of the corpus callosum. The white boxes indicate examples from regions of low (B) and high (C) expected anisotropy. (**B** and **C**) Each image subsection was windowed to reduce edge effects and the 2D Fourier transform (2DFT) was applied. Radial integration and principal component analysis was applied to derive anisotropy ($A_{er}$) and orientation ($\theta$). (**D**) The calculated orientation and anisotropy were displayed as hue and saturation, respectively, and the 2D ellipse was overlaid in white.

the lateral ventricles and corpus callosum, respectively. The mean length of tracks within each of the regions of interest was determined with TrackVis (Wang *et al.*, 2007). Additionally, 2D (in-plane) tractography procedure was performed for both the *ex vivo* DTI and tiled histological images. For both modalities, anisotropy was calculated as ($A_{er} = 1 - \lambda_2/\lambda_1$) where the through-plane (z) components of the diffusion tensor were set to zero. An $A_{er}$ threshold of 0.15 was used for the 2D *ex vivo* DTI and histological tractography, and the resulting tractography maps were used for qualitative comparison.

## Statistical analysis

The DTI parameters (fractional anisotropy, axial diffusivity or radial diffusivity) and the histological-derived anisotropy (scaled $A_{er}$) were compared among perilesional, contralateral and control tissues using one-way ANOVA separately for white and grey matter. *Post hoc* comparisons were performed with a Student's *t*-test if the overall model reached significance. A multiple linear regression analysis was employed to determine which of the histological stains best predicted each of the DTI parameters using a standard linear least squares. White and grey matter was tested in separate models. If the ANOVAs were significant, effect tests were performed for each of the regressors. All statistical tests were performed with JMP 8 (SAS Institute Inc.), and a *P*-value $<0.05$ was deemed significant.

# Results

## Increased cortical and decreased white matter fractional anisotropy following traumatic brain injury

At 2 months following controlled cortical impact, fractional anisotropy was increased in the cortex adjacent to the lesion compared with the contralateral cortex and control cortices (Fig. 1A). Table 1 contains a summary of the diffusion metrics (fractional anisotropy, radial diffusivity and axial diffusivity) and statistical analysis of DTI and histological measures between region of interest in controlled cortical impact and control rats. The primary axis of diffusion maintained its orientation perpendicular to the cortical surface, since the normal rodent cortex has a radially oriented anisotropy, albeit with a lower fractional anisotropy than white matter tracts. Across all animals (Fig. 1C), the cortex had a significantly main effect of fractional anisotropy ($P = 0.002$), with a significant increase in the perilesioned cortex compared with both the contralateral ($P < 0.001$) and control cortices ($P = 0.003$). The individual diffusivities oriented parallel (axial) or perpendicular (radial) to the main axis were also examined. Compared with control values, a significant increase in axial diffusivity was evident in the perilesioned cortex ($P < 0.001$), with no change in radial diffusivity. In the white matter consisting of the external capsule and corpus callosum, fractional anisotropy had a significant main effect ($P = 0.002$), with a significant decrease in the perilesioned region compared with contralateral ($P = 0.0102$) and control rats ($P < 0.001$). Radial diffusivity was significantly increased ($P = 0.0028$), whereas axial diffusivity was not significantly different compared with control rats.

## Whole-brain quantification and visualization of anisotropy from histological sections

A method to quantify the anisotropy of histological sections using Fourier analysis was developed and is depicted in Fig. 2 and described in Appendix I. Brain sections from a control rat were stained with the lipophilic dye DiI, and the colour-coded orientation and anisotropy maps were derived using the developed algorithm. The histology-derived maps were visually compared with the corresponding *ex vivo* DTI maps reconstructed without the through-plane (z) components, allowing for direct comparison (Fig. 3). *Ex vivo* DTI was used since it afforded greater resolution and signal to noise ratio than the *in vivo* DTI. Both modalities have strikingly similar features, with anisotropy highest in the white matter tracts, as expected, and the cortex displaying a clear radial orientation with lower anisotropy than that of the white matter fibres. The increase in anisotropy was not strictly limited to myelinated regions, since some of the thalamic and hypothalamic nuclei have appreciable anisotropy. Whereas the

**Table 1 Summary and statistical analysis of DTI and histological measures between regions**

| Measure | Lesion | Contralateral | Control | *F*-value (*P*-value) | Lesion versus contralateral *P*-value | Lesion versus control *P*-value | Contralateral versus control *P*-value |
|---|---|---|---|---|---|---|---|
| Grey matter | | | | | | | |
| FA | 0.31 ± 0.05 | 0.22 ± 0.03 | 0.24 ± 0.01 | 11.25 (0.002) | <0.001 | 0.003 | 0.53 |
| Axial | 1.05 ± 0.06 | 0.91 ± 0.05 | 0.96 ± 0.03 | 9.55 (0.003) | <0.001 | 0.02 | 0.15 |
| Radial | 0.66 ± 0.05 | 0.66 ± 0.02 | 0.67 ± 0.01 | 0.27 (0.77) | – | – | – |
| GFAP | 0.51 ± 0.22 | 0.11 ± 0.03 | 0.14 ± 0.03 | 15.44 (<0.001) | <0.001 | <0.001 | 0.73 |
| MAP2 | 0.11 ± 0.04 | 0.21 ± 0.08 | 0.18 ± 0.05 | 3.30 (0.072) | – | – | – |
| SMI31 | 0.15 ± 0.05 | 0.18 ± 0.06 | 0.10 ± 0.03 | 3.19 (0.077) | – | – | – |
| SMI32 | 0.12 ± 0.03 | 0.20 ± 0.07 | 0.19 ± 0.05 | 2.92 (0.092) | – | – | – |
| White matter | | | | | | | |
| FA | 0.40 ± 0.05 | 0.48 ± 0.05 | 0.51 ± 0.01 | 10.32 (0.002) | 0.0102 | <0.001 | 0.18 |
| Axial | 1.24 ± 0.10 | 1.18 ± 0.08 | 1.27 ± 0.04 | 1.82 (0.2) | – | – | – |
| Radial | 0.63 ± 0.06 | 0.53 ± 0.03 | 0.54 ± 0.02 | 8.45 (0.005) | 0.0028 | 0.0058 | 0.71 |
| GFAP | 0.59 ± 0.19 | 0.69 ± 0.29 | 0.39 ± 0.11 | 2.68 (0.11) | – | – | – |
| MBP | 0.08 ± 0.04 | 0.14 ± 0.03 | 0.15 ± 0.02 | 8.09 (0.006) | 0.0049 | 0.0042 | 0.93 |
| SMI31 | 0.43 ± 0.22 | 0.55 ± 0.23 | 0.27 ± 0.13 | 2.33 (0.14) | – | – | – |
| SMI32 | 0.31 ± 0.15 | 0.38 ± 0.07 | 0.20 ± 0.18 | 1.90 (0.19) | – | – | – |

Values indicate mean ± SD ($n = 5$ for each).
*F*-values were computed from a one-way ANOVA, and Student's *t*-test *post hoc* comparisons indicate *P*-values.
FA = fractional anisotropy (unitless); GFAP = glial fibrillary acidic protein; MBP = myelin basic protein; axial and radial ($\mu m^2$/ms).

DTI maps suffer from partial volume effects due to the averaging across 500 μm slices, the histology-derived maps were reconstructed from 8 μm sections and have a much sharper appearance.

## Gliosis is the primary correlate of increased cortical anisotropy

The developed method was applied to histological sections from controlled cortical impact and control brains to identify the specific cellular and subcellular features that give rise to the anisotropy changes in the cortex and white matter. A qualitative assessment is first shown in Fig. 4, with clear changes in the perilesioned cortex and white matter compared with the contralateral and control tissues. Notably, a pronounced increase in glial fibrillary acidic protein-positive astrocytes was evident in both the white and grey matter of the perilesioned cortex. Slight decreases in MAP2 and SMI32 content were also observed, indicative of dendritic injury. The anisotropy maps revealed that in the selected samples, anisotropy of glial fibrillary acidic protein, MAP2, SMI31, and SMI32 were all increased compared with the contralateral tissue, although the greatest change was observed with glial fibrillary acidic protein. In the white matter, the most notable changes were the decreased myelin basic protein and the increased SMI32, indicating demyelination and axonal injury, respectively. There was a decrease of anisotropy in the perilesioned white matter, specifically with myelin basic protein and SMI32. The group-averaged results from a region of interest analysis from all animals are shown in Fig. 5. A one-way ANOVA (Table 1) revealed a significant effect for the anisotropy (scaled $A_{er}$) of glial fibrillary acidic protein ($P < 0.001$), with the perilesioned cortex having a significant increase compared with both the contralateral ($P < 0.001$) and control ($P < 0.001$) cortices. In the white matter, myelin basic protein had a significant main effect ($P = 0.006$), with the perilesion region having a significantly lower scaled $A_{er}$ than either the control ($P = 0.0042$) or contralateral tissues ($P = 0.0049$). None of the other stains used were significantly different.

A multiple linear regression analysis was performed (Table 2) to quantify the degree to which the histological-derived anisotropy values predicted the measured DTI values. In the cortical grey matter, the anisotropy of the stained sections had a significant linear relationship with both fractional anisotropy (adjusted $r^2 = 0.54$, $P = 0.017$) and axial diffusivity (adjusted $r^2 = 0.64$, $P = 0.0055$). Specifically, glial fibrillary acidic protein had a significant positive relationship with fractional anisotropy (standardized $\beta = 0.62$, $P = 0.04$) and axial diffusivity ($\beta = 0.74$, $P = 0.0093$). In the white matter of the external capsule, both the fractional anisotropy (adjusted $r^2 = 0.59$, $P = 0.0096$) and radial diffusivity (adjusted $r^2 = 0.76$, $P < 0.001$) had a significant linear relationship with the anisotropy measured from the stained sections. Specifically, myelin basic protein ($\beta = 0.75$, $P = 0.0015$) and SMI32 ($\beta = -0.48$, $P = 0.043$) were significant predictors of fractional anisotropy. Myelin basic protein ($\beta = -0.86$, $P < 0.001$), SMI31 ($\beta = -0.49$, $P = 0.012$) and SMI32 ($\beta = 0.43$, $P = 0.021$) were also significantly related to radial diffusivity.

## Pathology of diffusion tensor tractography following traumatic brain injury

Whole-brain 3D DTI tractography was performed on the controlled cortical impact and control *in vivo* DTI volumes (Fig. 6).

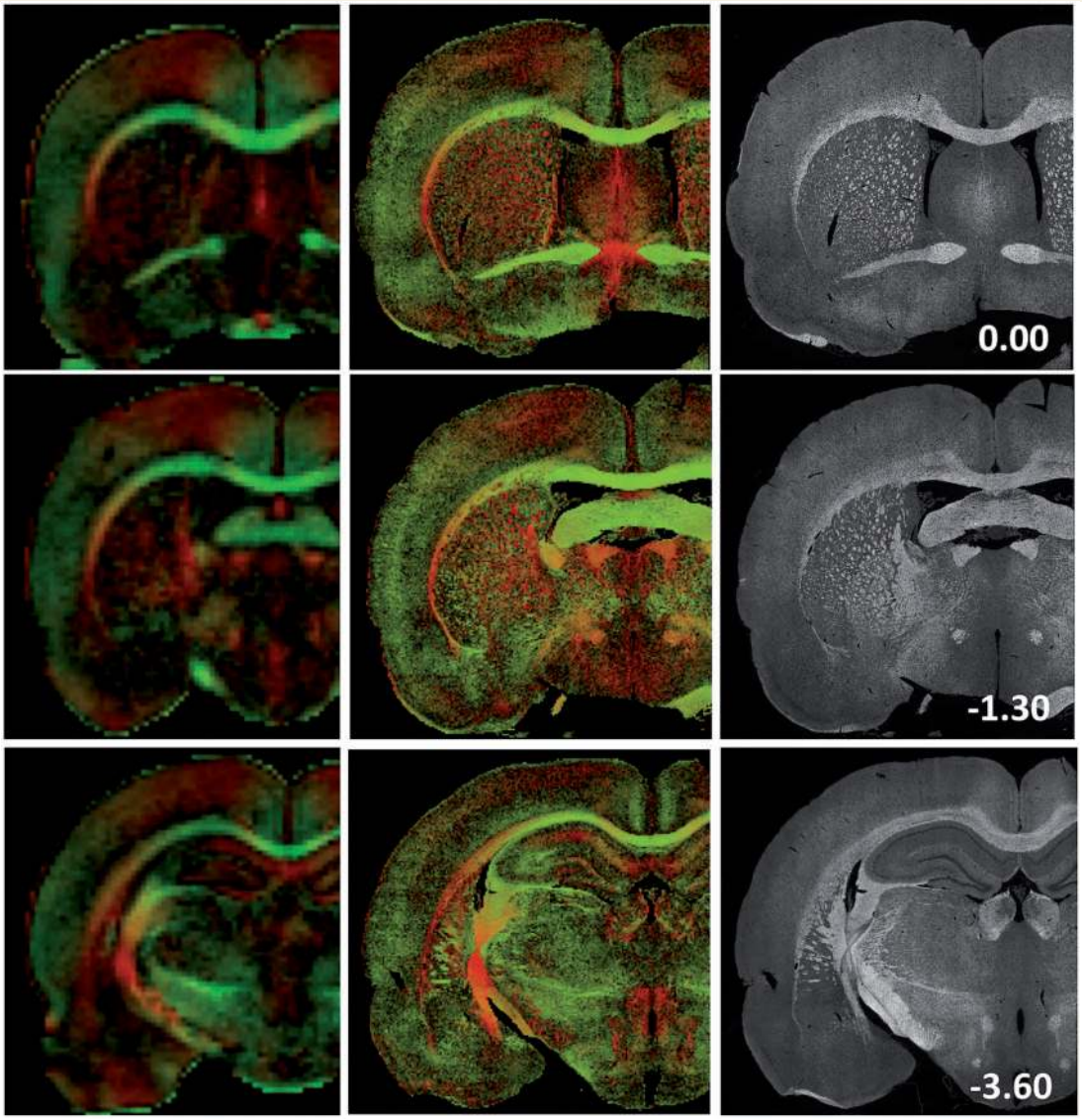


**Figure 3** Comparison of *ex vivo* DTI and whole-brain DiI sections. *Ex vivo* DTI maps colour-coded for anisotropy and orientation are shown for four slices from a control brain (*left*). The similarly coloured maps computed from the corresponding histological sections using the proposed method (*middle*) are similar in appearance to the DTI maps. The original DiI-stained sections are shown for reference (*right*), with the numbers indicating the anatomical location in reference to bregma.

In the controlled cortical impact brain, tracts originating in the external capsule and corpus callosum propagated into the lesioned cortex, whereas similar tracts were not observed in the control brain. Region of interest analysis was performed by segmenting regions of the cortex according to boundaries that included the cortical surface, lateral ventricles and corpus callosum (Fig. 6B). The mean length of tracts passing in the controlled cortical impact cortex was significantly greater ($t = 3.157$; $P = 0.034$) than that of the contralateral cortex (Fig. 6D).

In-plane (2D) tractography was performed on both the DTI images and the histological images for direct comparison. The *ex vivo* 3D diffusion tensor tractography from three separate animals (Fig. 7A) depicts tracts propagating along the lesion border and into the cortex, similar to the *in vivo* tractography (Fig. 6). To permit a direct comparison, diffusion tensor tractography was subsequently performed in 2D (Fig. 7B) and visually compared with the histology-derived tractography performed on the processed histological sections stained for glial fibrillary acidic protein and SMI32 (Fig. 7C and E). The glial fibrillary acidic protein-derived tracts were visually similar to those shown for DTI, with significant numbers of tracts propagating along the lesion periphery and into the cortex. The coherent orientation of astrocytes that gave rise to the increased tract density was evident in the confocal images (Fig. 7D). By comparison, tracts derived from SMI32 sections were less dense (Fig. 7E) and staining intensity was diminished (Fig. 7F), suggesting that few or no SMI32-positive axons or dendrites were maintained or had sprouted into the lesion at 30 days post injury.

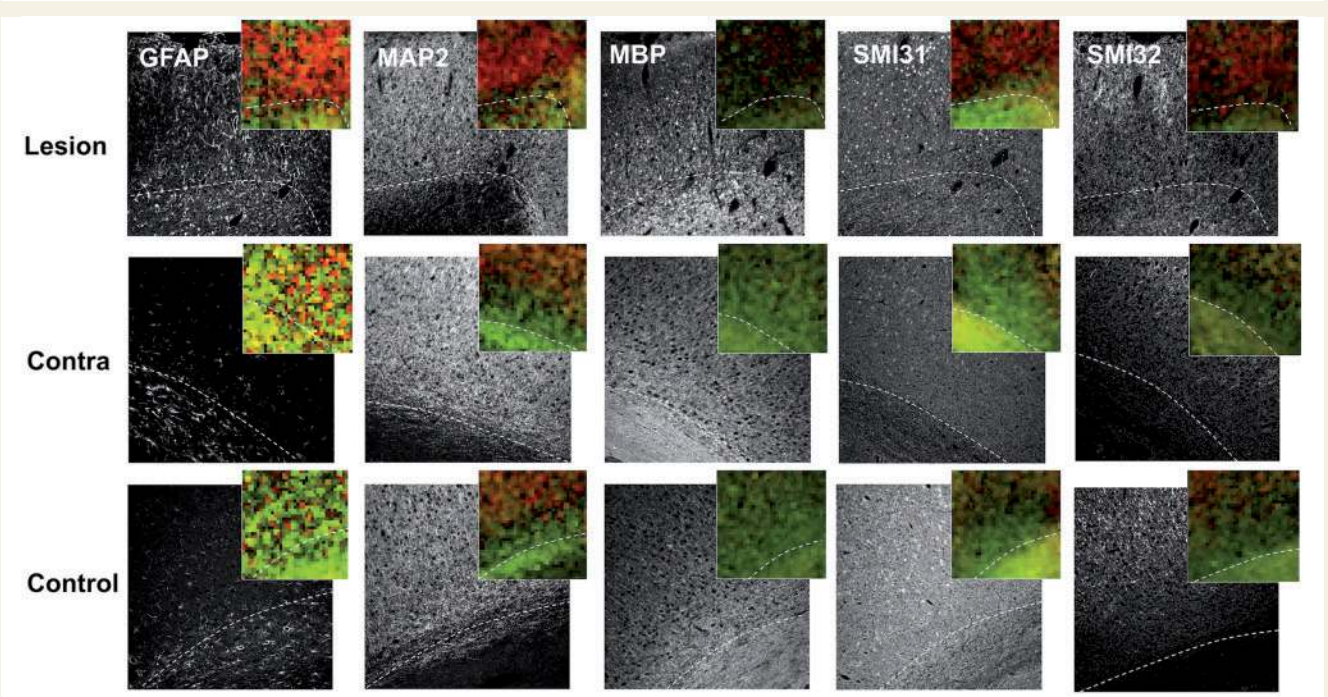


**Figure 4** Cellular components of controlled cortical impact lesions using immunofluorescence and anisotropy maps. Within the injured controlled cortical impact cortex and white matter, glial fibrillary acidic protein (GFAP)-positive astrocytes are prolific. In the cortex, lesser changes in MAP2, SMI31 and SMI32 were evident, with all four stains displaying increased anisotropy as shown in the $A_{er}$ maps (*insets*). In the white matter, increased SMI32 staining and decreased myelin basic protein (MBP) structural integrity were evident in both the stained sections and the resulting $A_{er}$ maps (*insets*).

# Discussion

DTI is exquisitely sensitive to microstructural abnormalities caused by trauma to the CNS that are not appreciated by conventional MRI (Kumar *et al.*, 2009). Fractional anisotropy is most often decreased in white matter following traumatic brain injury indicative of a loss of white matter integrity (Kumar *et al.*, 2009), but increased fractional anisotropy is occasionally seen (Sidaros *et al.*, 2008; Wilde *et al.*, 2008). In the current study, a novel approach to quantify the anisotropy of histological sections using Fourier analysis was directly compared with the results of anisotropy measured with DTI. The results indicate that the increased fractional anisotropy in the cortex following traumatic brain injury in a rat controlled cortical impact model is associated with coherent arrangement of reactive astrocytes, whereas the decreased fractional anisotropy in the white matter is related to demyelination and axonal degeneration.

The decreased white matter fractional anisotropy we observed at 2 months post-injury is consistent with the longitudinal study by MacDonald *et al*. (2007) in a mouse controlled cortical impact model. They demonstrated that white matter anisotropy was similarly decreased between 4 h and 1 month following the injury, but axial and radial diffusivity were differentially responsible for the fractional anisotropy decrease depending on the time after the injury. In the acute phase, axial diffusivity was decreased and was likely related to transient aspects of axonal injury, such as the formation of swellings (Dickson *et al.*, 2007) or beading (Budde and Frank, 2010). In the chronic phase, axial diffusivity returned to normal or supranormal values, whereas radial diffusivity was increased, consistent with demyelination and prolonged axonal degeneration (Song *et al.*, 2003). Thus, the DTI changes were associated with different microstructural features as the injury evolved. Our results in the white matter are consistent with previous reports demonstrating that the fractional anisotropy decrease is associated with demyelination, and to a lesser extent axonal degeneration. However, neuroinflammatory processes, including macrophage and microglia proliferation, are robust responses to traumatic brain injury (Raghavendra Rao *et al.*, 2000; Loane and Byrnes, 2010) and could also be a contributing factor since these pathologies have been related to fractional anisotropy changes in other injuries (Saadani-Makki *et al.*, 2009; Thiel *et al.*, 2010; Xie *et al.*, 2010). Although the axonal membrane is the major determinant of anisotropy in normal white matter (Beaulieu and Allen, 1994), diffusion anisotropy of injured white matter is multifaceted.

Astrocytes, which are largely responsible for maintaining homeostasis in the CNS, typically have extensive processes with a stellate morphology. Thus, they are traditionally viewed as macroscopically isotropic and would therefore either not affect anisotropy or reduce the measured anisotropy. However, two types of astrocytes have been reported, protoplasmic and fibrous, which have distinct morphologies and regional distributions (Wilhelmsson *et al.*, 2006; Oberheim *et al.*, 2008). The astrocytes of the normal cerebral cortex are predominantly protoplasmic astrocytes

that appear isotropic and maintain non-overlapping spatial domains (Wilhelmsson *et al.*, 2006; Oberheim *et al.*, 2008). Although some reports have indicated that protoplasmic astrocytes retain their distinct domains following injury in addition to becoming hypertrophic (isomorphic gliosis), other reports have shown that they can asymmetrically extend their processes in the direction of the lesion (Oberheim *et al.*, 2008), referred to as palisading, which gives rise to anisomorphic gliosis (Mansour *et al.*, 1990) and formation of a glial scar. In the current study, we demonstrated that this increased cohesiveness could give rise to increased grey matter anisotropy, which has been visualized previously (Schwartz *et al.*, 2005) and quantitatively demonstrated herein (Fig. 5). On the other hand, fibrous astrocytes are the primary type of astrocytes in white matter. These cells have intrinsically longer processes (Oberheim *et al.*, 2009) that are arranged parallel to white matter fibres in the normal brain (Bitner *et al.*, 1987) and interdigitate with one another (Sun *et al.*, 2010). Following injury, these cells in the white matter become hypertrophic like those of the cortex, but also have a propensity to migrate to the site of injury (Sun *et al.*, 2010). In the current study, the increase in astrocyte content combined with the directional cohesiveness gives rise to the increased cortical anisotropy as measured with DTI.

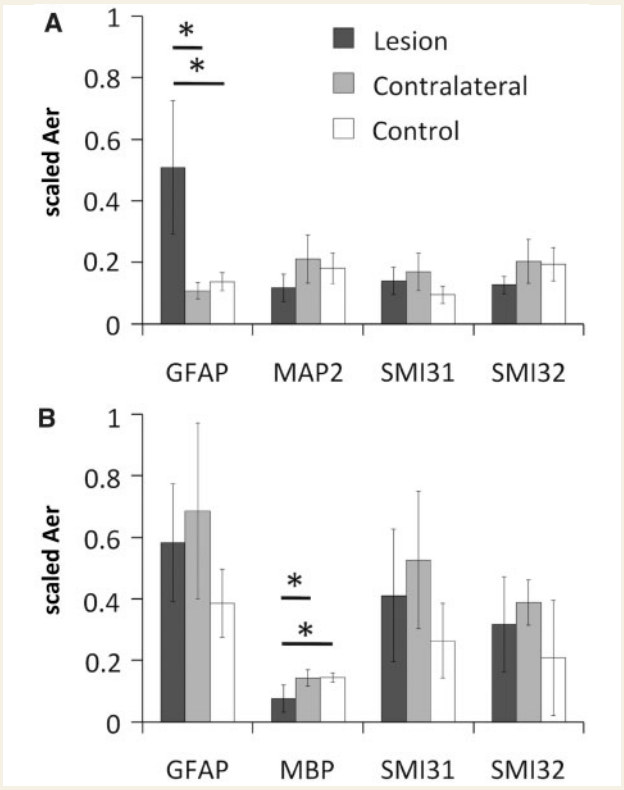


**Figure 5** Quantitative histology results. (**A**) In the cortex, glial fibrillary acidic protein (GFAP)-derived anisotropy was significantly greater in the perilesioned tissue compared with the contralateral and control cortices. (**B**) In the white matter, myelin basic protein (MBP) anisotropy was significantly decreased in the perilesioned tissue compared with the contralateral and control white matter. Values indicate mean ± SD ($n = 5$ for each). *$P < 0.05$.

The concept of axonal sprouting and regeneration following injury has important implications to the recovery of function (Dancause *et al.*, 2005). The CNS has a capacity for recovery through functional plasticity (Nishibe *et al.*, 2010), although the potential for extensive structural reorganization following injury is more limited (Cafferty *et al.*, 2008). The failure is largely attributed to factors within the lesion milieu that suppress outgrowth, although astrocyte proliferation has also been likened to functional recovery following injury (Keiner *et al.*, 2008). Sprouting of neurites is most often demonstrated in the injured, untreated brain using injectable axonal tracers (Steward *et al.*, 2003; Dancause *et al.*, 2005). However, without appreciable coherent organization, the sparse regrowth of individual axons through the existing neuropil (Lenzlinger *et al.*, 2005; Harris *et al.*, 2010) is unlikely to have a significant effect on anisotropy measurements over a scale of a DTI voxel (for this study *ex vivo* image resolution was 156 × 156 × 500 μm). Despite the disconnection between microstructural changes and DTI, increased fractional anisotropy is often interpreted as reorganization or regrowth of axons and dendrites

**Table 2 Multiple linear regression analysis of the histological predictors of DTI**

| Measure | Full model | | Standardized β (*P*-value) | | | |
|---|---|---|---|---|---|---|
| | Adjusted $r^2$ | *F*-ratio | Glial fibrillary acidic protein | MAP2 | SMI31 | SMI32 |
| Cortex | | | | | | |
| FA | 0.54 | 5.04 (0.017) | 0.62 (0.04) | −0.20 (0.36) | −1.21 (0.26) | −0.08 (0.74) |
| Axial | 0.64 | 7.14 (0.0055) | 0.74 (0.0093) | −0.04 (0.82) | −0.25 (0.2) | −0.10 (0.65) |
| Radial | −0.29 | 0.22 (0.92) | *Post hoc* comparisons not performed | | | |
| | | | Glial fibrillary acidic protein | Myelin basic protein | SMI31 | SMI32 |
| White matter | | | | | | |
| FA | 0.59 | 6.07 (0.0096) | 0.32 (0.14) | 0.75 (0.0015) | −0.07 (0.73) | −0.48 (0.043) |
| Axial | −0.09 | 0.70 (0.61) | *Post hoc* comparisons not performed | | | |
| Radial | 0.76 | 12.33 (<0.001) | 0.00 (0.99) | −0.86 (<0.001) | −0.49 (0.012) | 0.43 (0.021) |

*P*-values are indicated in parentheses.
FA = fractional anisotropy.

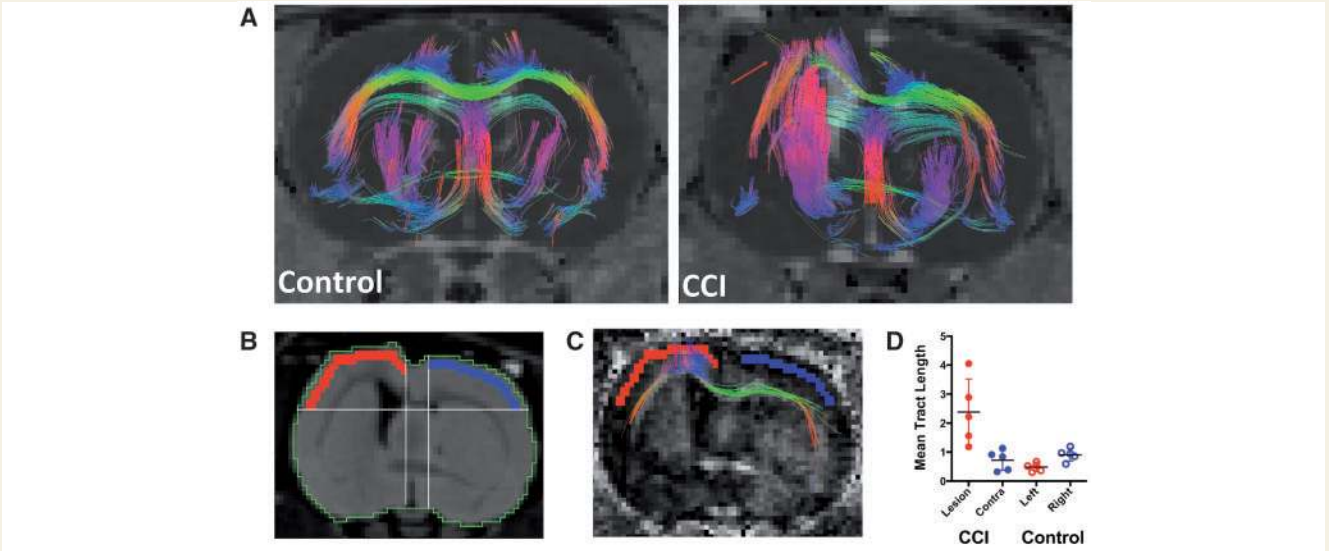


**Figure 6** Whole-brain *in vivo* DTI tractography. (**A**) DTI tractography of normal rat brain (*left*) and the controlled cortical impact (CCI) brain (*right*) reveals numerous tracts propagating into the controlled cortical impact lesion (arrow). (**B**) Regions of interest were segmented using boundaries that included the cortical surface (green), the medial aspect of the lateral ventricle and the posterior edge of the corpus callosum. (**C**) The region of interest mask applied to the tractography results demonstrates numerous tracts that course through both the cortical lesion and the corpus callosum. (**D**) Among all animals, the mean tract length of cortical tracts is significantly greater in the lesioned cortex compared with either the contralateral or control brain.

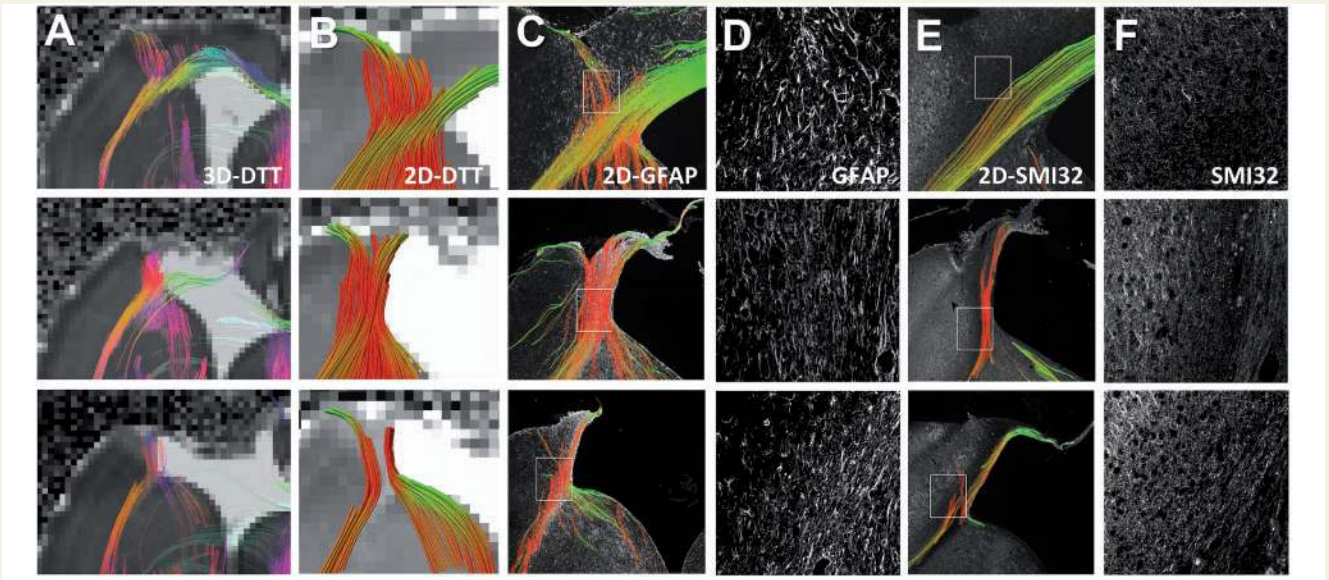


**Figure 7** Comparison of diffusion tensor tractography and histology-derived tractography. Three representative controlled cortical impact animals are shown. (**A**) *Ex vivo* 3D diffusion tensor tractography (DTT) maps depict tracts propagating in and along the lesion periphery similar to those observed *in vivo*. (**B**) 2D diffusion tensor tractography was subsequently performed to allow direct comparison to the 2D histology-derived tractography. (**C**) 2D tractography maps from the glial fibrillary acidic protein (GFAP)-stained sections revealed similarities to the DTI-derived maps near the lesion border. (**D**) The coherent orientation of astrocytes is shown on confocal images from selected regions. (**E**) 2D tractography maps from the SMI32-stained sections revealed fewer, if any, tracts propagating into the cortex near the lesion periphery. (**F**) A loss of structural integrity is noted for both the injured white matter and grey matter along the lesion border.

(Jiang *et al.*, 2006; Voss *et al.*, 2006; Ding *et al.*, 2008). In a rodent stroke model, increased fractional anisotropy in the ischaemic boundary was argued to reflect white matter reorganization, possibly in the form of axonal sprouting (Jiang *et al.*, 2006), but the authors previously showed that this region constituted a substantial glial scar in which no axonal regeneration was observed (Li *et al.*, 2005). Fractional anisotropy increases have been noted in the traumatically injured rat brain (Jiang *et al.*, 2011), but

the known prolific response of astrocytes (Dunn-Meynell and Levin, 1997) was neglected. The role of astrocytes on DTI has been appreciated in spinal cord injury (Schwartz *et al.*, 2005), hypoxia–ischaemia injury (Anderova *et al.*, 2010), dysmyelination (Harsan *et al.*, 2007) and radiation injury (Wang *et al.*, 2009), but the current study is the first to directly validate the changes by measuring the anisotropy of the underlying histological tissues.

The Fourier-based method of calculating anisotropy and orientation has been demonstrated for cultured cells (Marquez, 2006), bone tissues (Dziedzic-Goclawska *et al.*, 1982) and industrial applications (Josso *et al.*, 2005; Ayres *et al.*, 2008), and has its origins in optical diffraction experiments (Pernick *et al.*, 1978). We extended the method to mimic DTI-measured anisotropy using a pixelwise approach. Importantly, the method is automated, objective and does not necessitate manual tracing (Leergaard *et al.*, 2010) of axons or other structures, although validation with such techniques will be important (Bock *et al.*, 2010). Moreover, the method is applicable to either fluorescence or optical staining protocols. Another optical technique, polarized light imaging, has been used to measure anisotropy of brain tissues based on the birefringence of myelin sheaths (de Campos Vidal *et al.*, 1980; Axer *et al.*, 2011). Compared with that technique, the use of stained sections allows the different cellular and subcellular components to be evaluated independently of one another, since they have unique contributions to the water diffusion characteristics of tissues (Beaulieu, 2002).

One limitation of the proposed methodology is the lack of the third dimension, although this is a practical, and not theoretical, restriction. Thus, there is an obvious disparity between the thickness of the MRI slices and that of the histological sections. The DTI changes that we observed in the perilesioned region occurred over multiple slices of a 500 μm thickness, and in this study three adjacent slices were averaged for the DTI analysis. The histological sections were derived from the centre of the controlled cortical impact cortical lesion and it is believed that they sufficiently captured the pathology of the tissue of interest, since severe cortical injury occurs following controlled cortical impact (Dunn-Meynell and Levin, 1997). It should also be noted that in the current work, the primary direction of cortical and white matter anisotropy was oriented perpendicular to the coronal slices (Fig. 1), allowing the long-axis to be viewed in cross-section. This is not expected to be the case for all tissues of interest, and presents a limitation given the 2D nature of most histological preparations. Three-dimensional microscopy may aid in further validation studies by incorporating *z* stacks by confocal or multi-photon microscopy of thicker histological sections or *in vivo* systems. To account for the inherent 2D limitation, the tractography of the *ex vivo* DTI data was limited to in-plane analysis by setting the *z*-components of the diffusion tensor to zero. With appropriate care taken to ensure similar slice orientations between the two modalities and the comparison of the identical parameter $A_{er}$ (Pierpaoli and Basser, 1996), the tractography results for each of the techniques should be directly comparable. Visual comparison of the tractography maps from each of the modalities revealed that tracts projecting into the lesion were those induced by gliosis and not axons (Fig. 7). The results highlight an inherent limitation and potential confound of tractography in the injured brain and spinal cord in that it detects the point-to-point voxel-averaged primary direction of diffusion on a macroscopic scale (Johansen-Berg and Behrens, 2006), regardless of the underlying biophysical and microstructural causes.

Our results demonstrate that gliosis is a major component of the DTI changes following traumatic brain injury. However, there are other known causes of increased fractional anisotropy subsequent to injury, so extrapolation of the current findings should be considered in the context of other potential sources. Acquisition artefacts (Gallichan *et al.*, 2010, Ling *et al.*, 2011, Tournier *et al.*, 2011) and low signal-to-noise (Pierpaoli and Basser, 1996) can artificially bias anisotropy, and these possibilities should be first ruled out with appropriate controls. Fractional anisotropy can increase in response to cell swelling and the associated shift of bulk water from the intracellular to the extracellular compartment that occurs following acute ischaemia (Armitage *et al.*, 1998) and may occur acutely after traumatic brain injury (Bazarian *et al.*, 2007; Mayer *et al.*, 2010). Similarly, physical compression of brain tissue caused by mass effects from tumours, abscesses or intracranial haemorrhages are also causes of increased fractional anisotropy (Gupta *et al.*, 2010) that could occur following severe traumatic brain injury. Finally, in the human brain, fibres that intersect at different orientations, known as crossing fibres, have a measured anisotropy less than that of fibres with a single orientation due to the limitations of the single tensor model in resolving multiple intra-voxel fibre orientations (Wiegell *et al.*, 2000). Selective injury to one of these crossing fibre tracts may cause the measured anisotropy to increase (Douaud *et al.*, 2010). Crossing fibre regions are often shown to have extensive DTI abnormalities in traumatic brain injury (Rutgers *et al.*, 2008). It remains to be determined whether this is a complication of DTI or whether crossing fibres are particularly prone to injury due to the concentration of shear forces in these regions. Clearly, attributing DTI changes to a single pathological feature is not without complications. Nonetheless, in the subacute to chronic phase after traumatic injury, reactive gliosis and the formation of a glial scar are dominant pathologies, and it is likely that astrocytes significantly contribute to the anisotropy observed along the injury border and perilesioned tissue. The results are important for the correct interpretation of DTI findings in the injured CNS and will therefore have implications in patient management and prognosis in traumatic brain injury as well as the evaluation of existing or novel pharmacological or cellular therapies.


# Acknowledgements

We thank Dr Carlo Pierpaoli, Dr Peter Basser and Dr Evren Ozarslan for helpful comments and suggestions.

# Funding

The work was supported by the Intramural Research Programme at the National Institutes of Health Clinical Centre and the Centre for Neuroscience and Regenerative Medicine (300604-8.01-60855 to J.A.F.).

# References


Anderova M, Vorisek I, Pivonkova H, Benesova J, Vargova L, Cicanic M, et al. Cell death/proliferation and alterations in glial morphology contribute to changes in diffusivity in the rat hippocampus after hypoxia-ischemia. J Cereb Blood Flow Metab 2010; 31: 894–907.

Arfanakis K, Haughton VM, Carew JD, Rogers BP, Dempsey RJ, Meyerand ME. Diffusion tensor MR imaging in diffuse axonal injury. AJNR Am J Neuroradiol 2002; 23: 794–802.

Armitage PA, Bastin ME. Selecting an appropriate anisotropy index for displaying diffusion tensor imaging data with improved contrast and sensitivity. Magn Reson Med 2000; 44: 117–21.

Armitage PA, Bastin ME, Marshall I, Wardlaw JM, Cannon J. Diffusion anisotropy measurements in ischaemic stroke of the human brain. MAGMA 1998; 6: 28–36.

Axer M, Amunts K, Grässel D, Palm C, Dammers J, Axer H, et al. A novel approach to the human connectome: ultra-high resolution mapping of fiber tracts in the brain. NeuroImage 2011; 54: 1091–101.

Ayres CE, Jha BS, Meredith H, Bowman JR, Bowlin GL, Henderson SC, et al. Measuring fiber alignment in electrospun scaffolds: a user's guide to the 2D fast Fourier transform approach. J Biomater Sci Polym Ed 2008; 19: 603–21.

Bazarian JJ, Zhong J, Blyth B, Zhu T, Kavcic V, Peterson D. Diffusion tensor imaging detects clinically important axonal damage after mild traumatic brain injury: a pilot study. J Neurotrauma 2007; 24: 1447–59.

Beaulieu C. The basis of anisotropic water diffusion in the nervous system - a technical review. NMR Biomed 2002; 15: 435–55.

Beaulieu C, Allen PS. Water diffusion in the giant axon of the squid: implications for diffusion-weighted MRI of the nervous system. Magn Reson Med 1994; 32: 579–83.

Bitner C, Benjelloun-Touimi S, Dupouey P. Palisading pattern of subpial astroglial processes in the adult rodent brain: relationship between the glial palisading pattern and the axonal and astroglial organization. Brain Res 1987; 465: 167–78.

Bock AS, Olavarria JF, Leigland LA, Taber EN, Jespersen SN, Kroenke CD. Diffusion tensor imaging detects early cerebral cortex abnormalities in neuronal architecture induced by bilateral neonatal enucleation: an experimental model in the ferret. Front Syst Neurosci 2010; 4: 1–11.

Brody DL, Mac Donald C, Kessens CC, Yuede C, Parsadanian M, Spinner M, et al. Electromagnetic controlled cortical impact device for precise, graded experimental traumatic brain injury. J Neurotrauma 2007; 24: 657–73.

Budde MD, Frank JA. Neurite beading is sufficient to decrease the apparent diffusion coefficient after ischemic stroke. Proc Natl Acad Sci USA 2010; 107: 14472–7.

Bush TG, Puvanachandra N, Horner CH, Polito A, Ostenfeld T, Svendsen CN, et al. Leukocyte infiltration, neuronal degeneration, and neurite outgrowth after ablation of scar-forming, reactive astrocytes in adult transgenic mice. Neuron 1999; 23: 297–308.

Cafferty WB, McGee AW, Strittmatter SM. Axonal growth therapeutics: regeneration or sprouting or plasticity? Trends Neurosci 2008; 31: 215–20.

Concha L, Gross DW, Wheatley BM, Beaulieu C. Diffusion tensor imaging of time-dependent axonal and myelin degradation after corpus callosotomy in epilepsy patients. Neuroimage 2006; 32: 1090–9.

Cox CS Jr, Baumgartner JE, Harting MT, Worth LL, Walker PA, Shah SK, et al. Autologous bone marrow mononuclear cell therapy for severe traumatic brain injury in children. Neurosurgery 2011; 68: 588–600.

Dancause N, Barbay S, Frost SB, Plautz EJ, Chen D, Zoubina EV, et al. Extensive cortical rewiring after brain injury. J Neurosci 2005; 25: 10167–79.

de Campos Vidal B, Mello ML, Caseiro-Filho AC, Godo C. Anisotropic properties of the myelin sheath. Acta Histochem 1980; 66: 32–9.

Dickson TC, Chung RS, McCormack GH, Staal JA, Vickers JC. Acute reactive and regenerative changes in mature cortical axons following injury. Neuroreport 2007; 18: 283–8.

Ding G, Jiang Q, Li L, Zhang L, Zhang ZG, Ledbetter KA, et al. Magnetic resonance imaging investigation of axonal remodeling and angiogenesis after embolic stroke in sildenafil-treated rats. J Cereb Blood Flow Metab 2008; 28: 1440–8.

Douaud G, Jbabdi S, Behrens TE, Menke RA, Gass A, Monsch AU, et al. DTI measures in crossing-fibre areas: increased diffusion anisotropy reveals early white matter alteration in MCI and mild Alzheimer's disease. Neuroimage 2010; 55: 880–90.

Dunn-Meynell AA, Levin BE. Histological markers of neuronal, axonal and astrocytic changes after lateral rigid impact traumatic brain injury. Brain Res 1997; 761: 25–41.

Dziedzic-Goclawska A, Rozycka M, Czyba JC, Sawicki W, Moutier R, Lenczowski S, et al. Application of the optical Fourier transform for analysis of the spatial distribution of collagen fibers in normal and osteopetrotic bone tissue. Histochemistry 1982; 74: 123–37.

Gallichan D, Scholz J, Bartsch A, Behrens TE, Robson MD, Miller KL. Addressing a systematic vibration artifact in diffusion-weighted MRI. Hum Brain Mapp 2010; 31: 193–202.

Gupta RK, Srivastava S, Saksena S, Rathore RK, Awasthi R, Prasad KN, et al. Correlation of DTI metrics in the wall and cavity of brain abscess with histology and immunohistochemistry. NMR Biomed 2010; 23: 262–9.

Harris NG, Mironova YA, Hovda DA, Sutton RL. Pericontusion axon sprouting is spatially and temporally consistent with a growth-permissive environment after traumatic brain injury. J Neuropathol Exp Neurol 2010; 69: 139–54.

Harsan LA, Poulet P, Guignard B, Parizel N, Skoff RP, Ghandour MS. Astrocytic hypertrophy in dysmyelination influences the diffusion anisotropy of white matter. J Neurosci Res 2007; 85: 935–44.

Jiang Q, Qu C, Chopp M, Ding GL, Davarani SP, Helpern JA, et al. MRI evaluation of axonal reorganization after bone marrow stromal cell treatment of traumatic brain injury. NMR Biomed 2011; doi:10.1002/nbm.1667.

Jiang Q, Zhang ZG, Ding GL, Silver B, Zhang L, Meng H, et al. MRI detects white matter reorganization after neural progenitor cell treatment of stroke. Neuroimage 2006; 32: 1080–9.

Johansen-Berg H, Behrens TE. Just pretty pictures? What diffusion tractography can add in clinical neuroscience. Curr Opin Neurol 2006; 19: 379–85.

Josso B, Burton DR, Lalor MJ. Texture orientation and anisotropy calculation by Fourier transform and principal component analysis. Mech Syst Signal Pr 2005; 19: 1152–61.

Keiner S, Wurm F, Kunze A, Witte OW, Redecker C. Rehabilitative therapies differentially alter proliferation and survival of glial cell populations in the perilesional zone of cortical infarcts. Glia 2008; 56: 516–27.

Kim JJ, Gean AD. Imaging for the diagnosis and management of traumatic brain injury. Neurotherapeutics 2011; 8: 39–53.

Kumar R, Husain M, Gupta RK, Hasan KM, Haris M, Agarwal AK, et al. Serial changes in the white matter diffusion tensor imaging metrics in moderate traumatic brain injury and correlation with neuro-cognitive function. J Neurotrauma 2009; 26: 481–95.

Leergaard TB, White NS, De Crespigny A, Bolstad I, D'arceuil H, Bjaalie JG, et al. Quantitative histological validation of diffusion MRI fiber orientation distributions in the rat brain. PLoS ONE 2010; 5: e8595.

Lenzlinger PM, Shimizu S, Marklund N, Thompson HJ, Schwab ME, Saatman KE, et al. Delayed inhibition of Nogo-A does not alter injury-induced axonal sprouting but enhances recovery of cognitive function following experimental traumatic brain injury in rats. Neuroscience 2005; 134: 1047–56.

Li Y, Chen J, Zhang CL, Wang L, Lu D, Katakowski M, et al. Gliosis and brain remodeling after treatment of stroke in rats with marrow stromal cells. Glia 2005; 49: 407–17.

Ling J, Merideth F, Caprihan A, Pena A, Teshiba T, Mayer AR. Head injury or head motion? Assessment and quantification of motion artifacts in diffusion tensor imaging studies. Hum Brain Mapp 2011; doi:10.1002/hbm.21192.

Lo C, Shifteh K, Gold T, Bello JA, Lipton ML. Diffusion tensor imaging abnormalities in patients with mild traumatic brain injury and neurocognitive impairment. J Comput Assist Tomogr 2009; 33: 293–7.

Loane DJ, Byrnes KR. Role of microglia in neurotrauma. Neurotherapeutics 2010; 7: 366–77.

MacDonald CL, Dikranian K, Bayly P, Holtzman D, Brody D. Diffusion tensor imaging reliably detects experimental traumatic axonal injury and indicates approximate time of injury. J Neurosci 2007; 27: 11869–76.

Mansour H, Asher R, Dahl D, Labkovsky B, Perides G, Bignami A. Permissive and non-permissive reactive astrocytes: immunofluorescence study with antibodies to the glial hyaluronate-binding protein. J Neurosci Res 1990; 25: 300–11.

Marquez JP. Fourier analysis and automated measurement of cell and fiber angular orientation distributions. Int J Solid Struct 2006; 43: 6413–23.

Mayer AR, Ling J, Mannell MV, Gasparovic C, Phillips JP, Doezema D, et al. A prospective diffusion tensor imaging study in mild traumatic brain injury. Neurology 2010; 74: 643–50.

Nishibe M, Barbay S, Guggenmos D, Nudo RJ. Reorganization of motor cortex after controlled cortical impact in rats and implications for functional recovery. J Neurotrauma 2010; 27: 2221–32.

Oberheim NA, Takano T, Han X, He W, Lin JH, Wang F, et al. Uniquely hominid features of adult human astrocytes. J Neurosci 2009; 29: 3276–87.

Oberheim NA, Tian GF, Han X, Peng W, Takano T, Ransom B, et al. Loss of astrocytic domain organization in the epileptic brain. J Neurosci 2008; 28: 3264–76.

Pernick B, Kopp RE, Lisa J, Mendelsohn J, Stone H, Wohlers R. Screening of cervical cytological samples using coherent optical processing. Part 1. Appl Opt 1978; 17: 21–34.

Pierpaoli C, Basser PJ. Toward a quantitative assessment of diffusion anisotropy. Magn Reson Med 1996; 36: 893–906.

Raghavendra Rao VL, Dogan A, Bowen KK, Dempsey RJ. Traumatic brain injury leads to increased expression of peripheral-type benzodiazepine receptors, neuronal death, and activation of astrocytes and microglia in rat thalamus. Exper Neurol 2000; 161: 102–14.

Rutgers DR, Toulgoat F, Cazejust J, Fillard P, Lasjaunias P, Ducreux D. White matter abnormalities in mild traumatic brain injury: a diffusion tensor imaging study. AJNR Am J Neuroradiol 2008; 29: 514–9.

Saadani-Makki F, Kannan S, Makki M, Muzik O, Janisse J, Romero R, et al. Intrauterine endotoxin administration leads to white matter diffusivity changes in newborn rabbits. J Child Neurol 2009; 24: 1179–89.

Schwartz ED, Duda J, Shumsky JS, Cooper ET, Gee J. Spinal cord diffusion tensor imaging and fiber tracking can identify white matter tract disruption and glial scar orientation following lateral funiculotomy. J Neurotrauma 2005; 22: 1388–98.

Sidaros A, Engberg AW, Sidaros K, Liptrot MG, Herning M, Petersen P, et al. Diffusion tensor imaging during recovery from severe traumatic brain injury and relation to clinical outcome: a longitudinal study. Brain 2008; 131 (Pt 2): 559–72.

Song SK, Sun SW, Ju WK, Lin SJ, Cross AH, Neufeld AH. Diffusion tensor imaging detects and differentiates axon and myelin degeneration in mouse optic nerve after retinal ischemia. NeuroImage 2003; 20: 1714–22.

Steward O, Zheng B, Tessier-Lavigne M. False resurrections: distinguishing regenerated from spared axons in the injured central nervous system. J Comp Neurol 2003; 459: 1–8.

Sun D, Lye-Barthel M, Masland RH, Jakobs TC. Structural remodeling of fibrous astrocytes after axonal injury. J Neurosci 2010; 30: 14008–19.

Thiel A, Radlinska BA, Paquette C, Sidel M, Soucy JP, Schirrmacher R, et al. The temporal dynamics of poststroke neuroinflammation: a longitudinal diffusion tensor imaging-guided PET study with 11C-PK11195 in acute subcortical stroke. J Nucl Med 2010; 51: 1404–12.

Tournier JD, Mori S, Leemans A. Diffusion tensor imaging and beyond. Magn Reson Med 2011; 65: 1532–56.

Voss HU, Uluc AM, Dyke JP, Watts R, Kobylarz EJ, McCandliss BD, et al. Possible axonal regrowth in late recovery from the minimally conscious state. J Clin Invest 2006; 116: 2005–11.

Wang R, Benner T, Sorensen AG, Wedeen VJ. Diffusion toolkit: a software package for diffusion imaging data processing and tractography. Proc Intl Soc Mag Reson Med 2007; 15: 3720.

Wang S, Wu EX, Qiu D, Leung LHT, Lau H-F, Khong P-L. Longitudinal diffusion tensor magnetic resonance imaging study of radiation-induced white matter damage in a rat model. Cancer Res 2009; 69: 1190–8.

Wiegell MR, Larsson HB, Wedeen VJ. Fiber crossing in human brain depicted with diffusion tensor MR imaging. Radiology 2000; 217: 897–903.

Wilde EA, McCauley SR, Hunter JV, Bigler ED, Chu Z, Wang ZJ, et al. Diffusion tensor imaging of acute mild traumatic brain injury in adolescents. Neurology 2008; 70: 948–55.

Wilhelmsson U, Bushong EA, Price DL, Smarr BL, Phung V, Terada M, et al. Redefining the concept of reactive astrocytes as cells that remain within their unique domains upon reaction to injury. Proc Natl Acad Sci USA 2006; 103: 17513–8.

Xie M, Tobin JE, Budde MD, Chen CI, Trinkaus K, Cross AH, et al. Rostrocaudal analysis of corpus callosum demyelination and axon damage across disease stages refines diffusion tensor imaging correlations with pathological features. J Neuropathol Exp Neurol 2010; 69: 704–16.

# Appendix I

The calculation of anisotropy and orientation of greyscale images using Fourier analysis was implemented based on previous descriptions (Josso *et al.*, 2005; Marquez, 2006). An image of size $M \times N$ is related to the frequency components by the 2D discrete Fourier transform

$$F(u,v) = \sum_{x=0}^{M-1}\sum_{y=0}^{N-1} f(x,y)e^{-i2\pi(ux/M + vy/N)}$$

where $x$ and $y$ represent the spatial coordinates of the image, $u$ and $v$ the frequency components along $x$ and $y$, and $i = \sqrt{-1}$. To remove edge effects that cause horizontal and vertical stripes in the Fourier domain, the image was multiplied with a 2D Tukey (tapered cosine) window in the spatial domain given by

$$\omega_0 = \begin{Bmatrix} 1 & r < \frac{(1-\alpha)N+1}{2} \\ \frac{1}{2}\left[1 + \cos\left(\pi\left(\frac{2r-1}{\alpha N} - \frac{1}{\alpha} + 1\right)\right)\right] & \frac{(1-\alpha)N+1}{2} \le r < \frac{N+1}{2} \\ 0 & \frac{N+1}{2} \le r \end{Bmatrix}$$

where $\alpha$ is the degree of taper $0 \leqslant \alpha \leqslant 1$, and $r$ is defined as

$$r = \sqrt{(x - \frac{N-1}{2})^2 + (y - \frac{N-1}{2})^2}$$

where for simplicity we assumed $N = M$ is an odd number. The power spectrum is given by

$$P(u,v) = \left|F(u,v)\right|^2 = R^2(u,v) + I^2(u,v)$$

where $R(u,v)$ and $I(u,v)$ are the real and imaginary values. The power spectrum can be expressed in polar coordinates of radial

frequency $u_r = \sqrt{u^2 + v^2}$ and angle $\theta = \tan^{-1}\frac{v}{u}$ by

$$P(u_r,\theta) = \left|F(u_r,\theta)\right|^2$$

The summation of power in a radial band of frequencies (annulus) intersecting an angular band (arc) is given by

$$A(\theta) = \sum_{u_r=f_c-f_w}^{f_c+f_w} \sum_{\theta=a_c-a_w}^{a_c+a_w} P(u_r,\theta)$$

where $f_c$ and $f_w$ are the centre and width of the annulus, and $a_c$ and $a_w$ are the centre and width of the arc, respectively. Conversion of the $n$ radial summations with angular widths (bin sizes) of $2\pi/n$ to Cartesian space yielded a $2 \times n$ data matrix of $x$ and $y$ point coordinates

$$X = \begin{bmatrix} A(u_1)\cdot\cos(\theta_1) & \cdots & A(u_n)\cdot\cos(\theta_n) \\ A(u_1)\cdot\sin(\theta_1) & \cdots & A(u_n)\cdot\sin(\theta_n) \end{bmatrix}$$

Principal component analysis performed using Eigen decomposition of the covariance matrix $C = XX^T$ resulted in two eigenvectors corresponding to the eigenvalues $\lambda_1$ and $\lambda_2$, where $\lambda_1 \geqslant \lambda_2$. The orientation of the first principal component in the spatial domain is specified by the polar angle $\theta_{pc1} = \tan^{-1}(v_{12}/v_{11})$, accounting for the $\pi/2$ rotation between the Fourier and spatial domains, where $v_{11}$ and $v_{12}$ are the components of the principal direction. Anisotropy is calculated as the eigenvalue ratio $A_{er} = 1 - (\lambda_2/\lambda_1)$.